Supporting Information

A Contactless Method for Measuring the Redox Potentials of Metal Nanoparticles

Randy Espinoza [#], Daniel Valenzuela Cahua [#], Kyle Magro, Son C. Nguyen *

Department of Chemistry and Biochemistry, University of California Merced, 5200 North Lake Road, Merced, California 95343, United States.

*Email: son@ucmerced.edu
# R.E. and D.V.C contributed equally to this work

Chemicals and Materials

All purchased reagents were used without any further purification. L-Ascorbic acid (AA, >99%), gold(III) chloride trihydrate ($HAuCl_4 \cdot 3H_2O$, 99.995%), 1,10-phenanthroline (PT, ≥99%), and sodium borohydride ($NaBH_4$, 99.99%) were purchased form Sigma-Aldrich. Ammonium iron(II) sulfate hexahydrate ($(NH4)_2Fe(SO_4)_2 \cdot 6H_2O$, 99%), cetyltrimethylammonium bromide (CTAB, >98.0%), and cetyltrimethylammonium chloride (CTAC, >95.0%) were purchased from Tokyo Chemical Industry Co., Ltd. Iron(III) chloride hexahydrate ($FeCl_3 \cdot 6H_2O$, 99+%), hydroxylamine hydrochloride ($NH_2OH \cdot HCl$, 99+%), and potassium bromide (KBr, reagent ACS) were purchased from Acros. Hydrochloric acid (HCl, 36.5%, 99.999% trace metal basis) was purchased from Alfa Aesar. Acetic acid (99.9%) and sodium acetate (≥99.7%) were purchased from Fisher Scientific. All water used for the synthesis of the gold nanoparticles and their reactions was purified using the Milli-Q IQ7000 system.

Instrumentation

The synthesized gold nanospheres were characterized using a FEI TALOS F200C G2 transmission electron microscope (TEM) operated at 200 kV. The reaction kinetics were monitored using UV−vis spectrometers (Ocean Optics, Maya 2000 Pro or USB 4000). The reaction mixtures were prepared in 1 cm path length quartz cuvettes from Spectrocell (R- 3010-T). Caps with an opening on top were used to seal the cuvettes with rubber septa. The samples were then purged using nitrogen gas on a Schlenk line to get rid of oxygen.

Synthesis of gold nanoparticles via seed-mediated growth method

Gold nanoparticles of different sizes were synthesized by following the procedures reported by Zheng and coworkers except that the volumes were scaled up by 20 times to obtain more particles per synthesis.[1] For the size of 74 nm, we found that the modified procedure from Lee and coworkers offered better size and shape distributions probably because the slightly excess amount of $AuCl_4^-$ etched and smoothed out the particles into spheres.[2] The average sizes characterized by TEM are 4.4 ± 0.6, 8.6 ± 0.5, 10.9 ± 0.5, 33 ± 1, 52 ± 2 nm, and 74 ± 3 nm (Figure S1).

Synthesis of CTAB-stabilized Au clusters

The Au clusters were prepared by rapidly adding 0.6 mL of fresh 10 mM $NaBH_4$ aqueous solution into a rapidly stirring (900 rpm) 10 mL solution of 0.25 mM $HAuCl_4$ and 100 mM CTAB using a pipette. Once mixed, the stirring speed of the now brown solution was reduced to 300 rpm for 2 minutes. After 2 minutes, stirring was turned off and the solution was kept undisturbed at ~27 °C for 3 h to allow the complete decomposition of excess $NaBH_4$ in the reaction mixture. These Au clusters were used as seeds to grow the 4.4, 8.6, and 10.9 nm gold nanoparticles.

Synthesis of the 4.4, 8.6, and 10.9 nm gold nanoparticles

The gold nanoparticles were grown by mixing 40 mL of 200 mM CTAC, 30 mL of 100 mM AA, and a given amount of the CTAB-capped Au seeds into a clean 250 mL Erlenmeyer flask. **The amount of seed solution added was 10 mL, 2 mL, and 0.9 mL for the 4.4, 8.6, and 10.9 nm gold nanoparticles, respectively.** Then, under vigorous stirring (700 rpm) 40 mL of 0.5 mM $HAuCl_4$ was quickly added all at once. After 15 minutes, a deep red solution developed and the gold nanoparticles were collected by centrifugation at 11,000 rpm for 30 minutes and washed with 20 mM CTAC three times for further use. For characterization, they were washed one additional time with water. Gold nanoparticles with a 10 nm diameter were dispersed in 20 mL of aqueous 20 mM CTAC solution and used as seeds for growing larger gold nanoparticles.

Synthesis of the 33, 52, and 74 nm gold nanoparticles

The larger gold nanoparticles were grown by mixing aqueous solutions of 40 mL of 20 mM CTAC, 2.2 mL of 10 mM AA and the 10 nm seeds were mixed in a 250 mL Erlenmeyer flask, followed by dropwise addition of aqueous 40 mL of 0.5 mM $HAuCl_4$ solution using a syringe pump at an injection rate of 40 mL h^{-1}. **The amount of 10 nm gold nanoparticle seed solution added was 0.510 mL, 0.188 mL, and 0.080 mL for the 33, 52, and 74 nm gold nanoparticles, respectively.** After all of the $HAuCl_4$ solution was injected, the reaction was allowed to continue for an additional 10 minutes. For the 74 nm gold nanoparticles, 2.2 mL of 10 mM AA was used and the reaction time was extended by 1 hour to allow excess $HAuCl_4$ to etch the gold nanoparticles into uniform spheres. The final product was collected by centrifugation at 11,000 rpm for 10 min and then washed with 20 mM CTAC three times for further use. For characterization, they were washed one additional time with water.

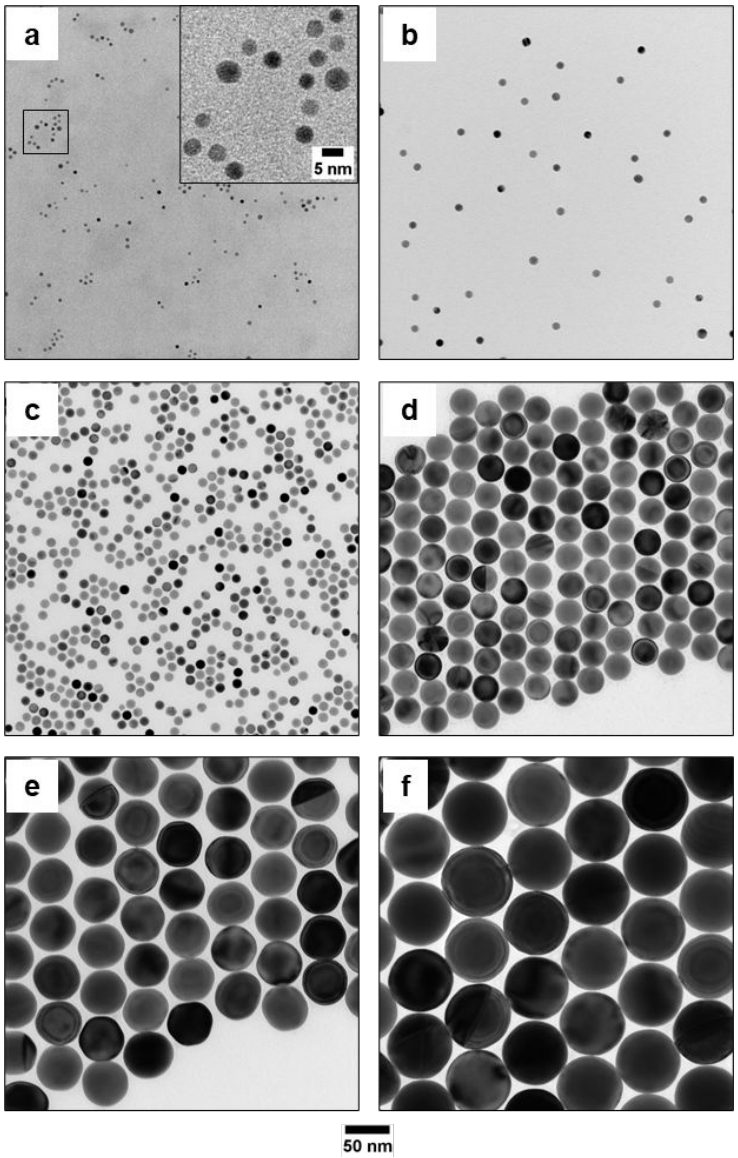

Figure S1. Representative TEM images of 4.4 nm (a), 8.6 nm (b), 10.9 nm (c), 33 nm (d), 52 nm (e), and 74 nm (f) gold nanoparticles prepared for this study. Inset in panel (a) is an enlarged cutout for better visualization.

Typical redox reactions between the gold nanoparticles and $FeCl_3$, and their conditions to reach reaction equilibria

In a 1 cm path length cuvette, an aliquot of gold nanoparticles (25 μL to 385 μL, depending on the size of the particles) with a specific diameter in the range of 4.4 nm to 74 nm suspended in 20 mM CTAC stock solution, 1.1 mL of 2 mM CTAB with added HCl to have a pH of 1.75, and Milli-Q water were added to bring the total volume to 1.875 mL. The reaction mixture was sealed with a rubber septum and purged with N_2 gas for 20 minutes under stirring. Lastly, the reaction was initiated by adding 0.125 mL of de-aerated 4.27 mM $FeCl_3$ to the mixture at room temperature in the absence of light. Note, a 50 mL of the 4.27 mM $FeCl_3$ stock solution was acidified with 100 μL of 12 M (36.5%) HCl to prevent hydrolysis. A list of the volumes of reactants used in the

reactions are shown in Table S1. The initial concentration of the gold nanoparticles was maintained approximately in the range of 0.2 – 0.25 mM of total Au(0) in the reaction solution, which is equivalent to an optical absorbance of 0.7 ~ 1.0 OD (1 cm path length) at the plasmon resonance peak. UV-vis spectra of the reactions of each particle size were recorded at various time intervals until they did not change, indicating the equilibria of the reactions (Figure S2). Since the initial pH of the reaction is 2 and the amount of ions in the reaction is small, this pH maintained the same during the reaction, preventing hydrolysis of iron ions. The clean background of spectra in Figure S2 also indicates no formation of insoluble iron hydroxides.

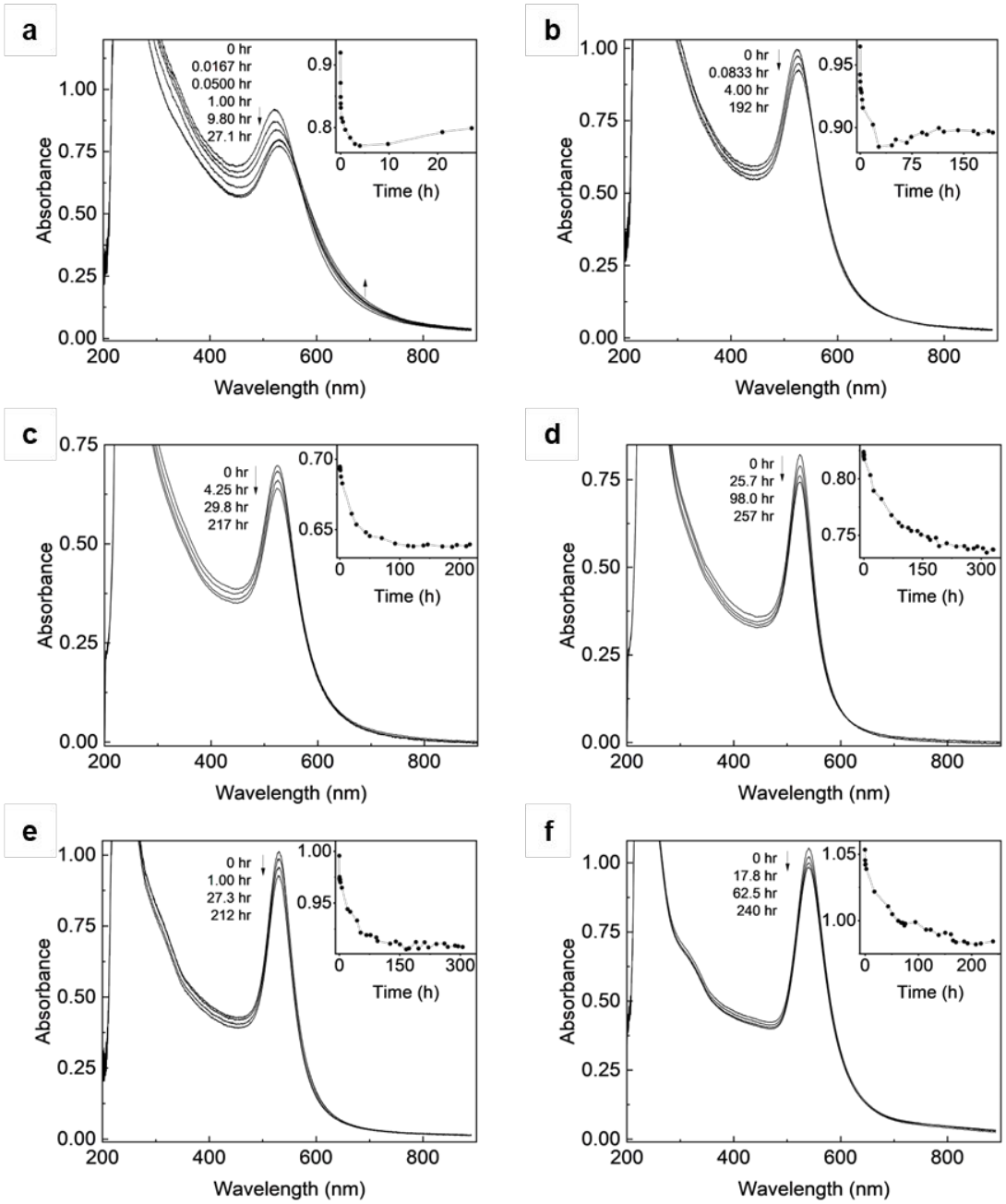

Figure S2. Representative UV-Vis absorption spectra at different time points for the $FeCl_3$ etching reaction of 4.4 nm (a), 8.6 nm (b), 10.9 nm (c), 33 nm (d), 52 nm (e), and 74 nm (f) gold

nanoparticles. The inset in each spectrum is the corresponding kinetic traces monitored by the localized surface plasmon resonance peak of the particles.

Redox reactions between the gold nanoparticles and $FeCl_3$ when the CTA^+ concentration was below, then raised above CMC

In a 1 cm path length cuvette, 100 μL of 11 nm gold nanoparticles suspended in 1 mM CTAC solution, 100 μL 1 mM CTAC, 1.1 mL of 2 mM KBr, 200 μL of 100 mM HCl, and 375 μL of Milli-Q water were added to bring the total volume to 1.875 mL. The reaction mixture was sealed with a rubber septum and purged with N_2 gas for 20 minutes under stirring. Lastly, 125 μL of de-aerated 4.27 mM $FeCl_3$ was added, and the UV-vis absorption spectrum of the reactions were recorded at different time intervals. After 70 hrs, 38 μL of de-areated 100 mM CTAC was carefully added to the reaction mixture using a syringe and continued monitoring the reaction at different time intervals until they reached equilibrium.

Redox reactions between the gold nanoparticles and $FeCl_3$ at different CTA^+ concentrations above CMC

In a 1 cm path length cuvette, 73 μL of 31.7 nm gold nanoparticles suspended in 20 mM CTAC solution was added to 1.1 mL of 2 mM CTAB with added HCl to have a pH of 1.75, 134 μL to 580 μL of different concentrations of CTAC (10 mM or 80 mM), and aliquots of Milli-Q water (122 μL to 568 μL) to bring the total volume to 1.875 mL. Note that the 31.7 nm size was conveniently selected for its availability in our lab. The reaction mixture was sealed with a rubber septum and purged with N_2 gas for 20 minutes under stirring. Lastly, 125 μL of de-aerated 4 mM $FeCl_3$ was added, and the UV-vis absorption spectrum of the reactions were monitored at different time intervals. Once the reaction is at equilibrium, the concentrations of $[Fe^{2+}]$ at equilibrium are measured through the phenanthroline assay (Figure S6).

Table S1. Typical reaction conditions between the gold nanoparticles and $FeCl_3$

Initial size (nm)	AuNPs in 20mM CTAC (μL)	2mM CTAB pH 1.75 (mL)	H_2O (μL)	4.27 mM $FeCl_3$ (μL)	20 mM CTAC (μL)
4.4	385	1.1	390	125	-
8.6	200	1.1	575	125	-
10.9	155	1.1	535	125	85
33	111	1.1	535	125	129
52	130	1.1	645	125	-
74	25	1.1	750	125	-

Determination of $[Fe^{3+}]$, $[Fe^{2+}]$, $[Au^+]$, and $[Br^-]$ at the equilibrium

The concentrations of chemicals at the equilibrium points of the reaction between gold nanoparticles and Fe^{3+} were determined as follows.

$[Fe^{2+}]$ in a reaction mixture was analyzed through the phenanthroline procedure as reported in our previous work.[3] Briefly, a standard curve was first built using standard solutions of $(NH_4)_2Fe(SO_4)_2$ with concentration range from 7.2 to 58.9 μM. First, in a 50 mL volumetric flask half full with water, a proper amount of stock $(NH_4)_2Fe(SO_4)_2$ (0.358 mM) solution was added followed by 5 mL of sodium acetate buffer (0.735 M in 1.566 M acetic acid), 1 mL of $NH_2OH{\cdot}HCl$ (0.144 M), and 2.5 mL of phenanthroline (11.1 mM). The solution was diluted to 50 mL using Milli-Q water. The absorbance at 511 nm of each standard solution was plotted against its concentration to obtain the molar extinction coefficient for the Fe(phenanthroline)$_3^{2+}$ complex.

Analysis of Fe^{2+} in the equilibrated reactions was performed in a similar manner as the standards. First, 1 mL of the reaction solution was centrifuged to separate the gold nanoparticles from the solution. After separating the supernatant from the gold nanoparticles sediment, 200 μL of the supernatant was transferred into a 1-cm pathlength cuvette containing 200 μL of the acetate buffer and 100 μL of the phenanthroline solution and brought up to 2 mL with Milli-Q water. The UV-Vis spectrum of the mixture was recorded and the absorbance value at 511 nm was used to calculate $[Fe^{2+}]$ through the standard curve. The calculated concentration was multiplied by 10 to get $[Fe^{2+}]$ in the equilibrium reaction mixture. $[Fe^{3+}]$ at equilibrium was calculated by subtracting its initial concentration by $[Fe^{2+}]$. Since $[Fe^{2+}]$ and $[AuBr_2^-]$ are stoichiometrically equal in this reaction, the $[AuBr_2^-]$ was taken to be the same as $[Fe^{2+}]$ at equilibrium. Finally, the $[Br^-]$ at equilibrium is calculated by taking the difference of its initial concentration and the amount consumed during the complexation with Au^+, which is twice the $[AuBr_2^-]$ at equilibrium.

Qualitative analysis of Au^+ and Au^{3+} in equilibrated reaction mixtures (after centrifuge to separate gold nanoparticles) were preformed based on previous literature. The assay was performed as follows: 200 μL of the reaction mixture was transferred to a 2-mm pathlength cuvette and added 10 μL of concentrated phosphoric acid (85%) to "shield" the yellow color of $FeBr_4$ and $FeCl_3$ as phosphoric acid forms a colorless complex with Fe^{3+}. Then , 200 uL of CTAB (100 mM) was added to the 200 μL reaction mixture in the cuvette and a second spectrum was recorded. Judging by the presence or absence of the Au^{3+}-CTAB complex absorption peak at ~ 390 nm, the presence or absence of Au^{3+} in the equilibrium reaction mixture can be tested. In all the reactions, Au^{3+} was not detected. As for the qualitative test of Au^+, 100 uL of 30% hydrogen peroxide was added to equilibrated reaction mixtures. The solution immediately turned yellow with the appearance of an absorption peak at 390 nm, which is due to the oxidation of Au^+ to Au^{3+} by hydrogen peroxide. The Au^{3+} and Au^+ tests proved that the etching product at equilibrium was Au^+ instead of Au^{3+}, which is consistent with previous reports[4]

Although $[Au^+]$, in the form of $AuBr_2^-$, was determined by the change in absorbance of gold nanoparticles, this method has low accuracy. A previous study[5] and our control experiments showed that the gold ion product adsorbed on the nanoparticles and alter their optical extinction. Consequently, we opt to use $[Fe^{2+}]$ for the equivalence value of $[Au^+]$ due to the high accuracy of the phenanthroline procedure.

Control reaction in the absence of gold nanoparticles

In a 1 cm path length cuvette, 1.1 mL of 2 mM CTAB with added HCl to have a pH of 1.75, and Milli-Q water were added to bring the total volume to 1.875 mL. The reaction mixture was sealed with a rubber septum and purged with N_2 gas for 20 minutes under stirring. Lastly, it was added 0.125 mL of de-aerated 4.27 mM $FeCl_3$ to the mixture at room temperature in the absence of light. After 27 hours, which is the time that 4.4 nm gold nanoparticles require to approach equilibrium under Fe^{3+} etching, analysis of Fe^{2+} through the phenanthroline procedure as previously described (Figure S3). No Fe^{2+} is observed using the phenanthroline procedure, indicating no Fe^{2+} forms in the absence of gold nanoparticles.

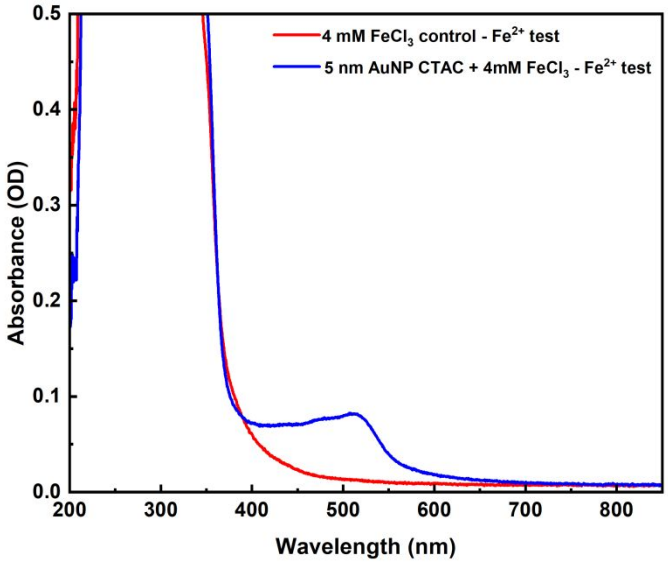

Figure S3. UV-Vis absorption spectra of phenanthroline assay for the $FeCl_3$ etching with 4.4 nm gold nanoparticles (blue) and a control reaction (red) after 27 hours.

Determination of gold nanoparticle size at the reaction equilibrium

At reaction equilibrium, the average sizes characterized by TEM are 5.0 ± 0.9, 8.7 ± 0.6, 10.2 ± 0.4, 31.9 ± 0.8, 50 ± 2, 73 ± 3 nm (Figure S4)

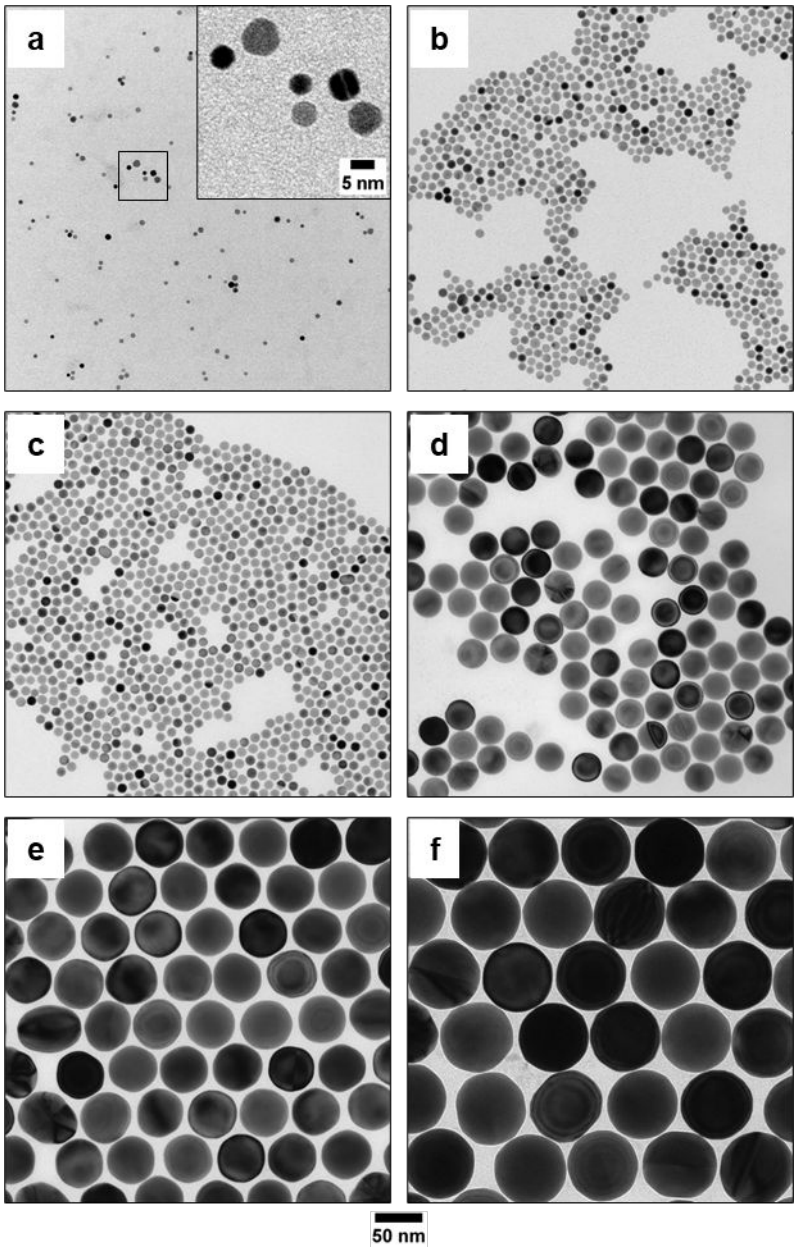

Figure S4. Representative TEM images of gold nanoparticles at reaction equilibrium. Their sizes are: 5.0 nm (a), 8.7 nm (b), 10.2 nm (c), 31.9 nm (d), 51 nm (e), and 73 nm (f). Their initial sizes are shown in Figure S1.

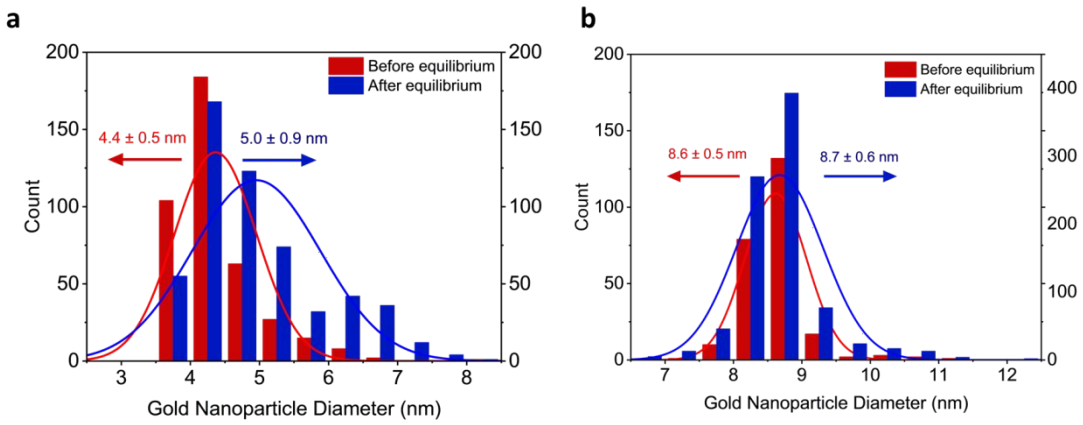

Figure S5. Size distributions of the two smallest nanoparticle samples before and at equilibria. The slight increase in particle sizes is the result of Oswalt ripening. The average sizes were extracted from a normal distribution fitting.

Using Nernst equation to determine standard reduction potential of gold nanoparticles

+ Determination of formal reduction potential $E^{o\prime}_{CTA_{mic}AuBr_2/AuNP}$ and standard reduction potential $E^{o}_{CTA_{mic}AuBr_2/AuNP}$

As mentioned in the main text, the entire reaction system (equation (4)) can be treated as an electrochemical cell having two "half-cell" reactions. The half-cell reaction for oxidation is:

$$Au_n^{NP}(s) + 2Br^- + CTA^+_{mic} \rightarrow 1e^- + Au_{n-1}^{NP}(s) + CTA_{mic}AuBr_2$$

And the half-cell reaction for reduction is:

$$Fe^{3+} + 1e^- \rightarrow Fe^{2+}$$

Using the Nernst equation for equation (5) in the main text, the standard reduction potentials of gold nanoparticles when the gold ion product is in $CTA_{mic}AuBr_2$ form can be determined as follows:

$$E_{cell} = E_{CTA_{mic}AuBr_2/AuNP} - E_{Fe^{3+}/Fe^{2+}} = 0$$

At the equilibrium of reaction (4), the Nernst equation is in this form:

$$E_{cell} = E^o_{cell} - \frac{RT}{zF}\ln K = E^o_{reduction} - E^o_{oxidation} - \frac{RT}{zF}\ln K = 0$$

Note that $E^o_{reduction}$ and $E^o_{oxidation}$ are the standard reduction potentials. K is unknown in our experiment and can be determined from reaction equation (4) in the main text. Using the above Nernst equation with concentrations of involved species, the formal potentials can be determined as follows:

$$E^{0\prime}_{Fe^{3+}/Fe^{2+}} - E^{0\prime}_{CTA_{mic}AuBr_2/AuNP} - \frac{RT}{zF}\ln\frac{[CTA_{mic}AuBr_2][Fe^{2+}]}{[Fe^{3+}][Br^-]^2[CTA^+_{mic}]} = 0$$

$$E^{0\prime}_{CTA_{mic}AuBr_2/AuNP} = E^{\circ}_{Fe^{3+}/Fe^{2+}} - \frac{RT}{zF}\ln\frac{[CTA_{mic}AuBr_2][Fe^{2+}]}{[Fe^{3+}][Br^-]^2[CTA^+_{mic}]} \qquad (S1)$$

Where $[CTA_{mic}AuBr_2]$ is assumed to be equal to $[AuBr_2^-]$ due to the favor product in equation (3). $[AuBr_2^-]$ is in turn equal to $[Fe^{2+}]$ due to equation (1). In control experiments when $[CTA^+]$ is above the critical micelle concentration (CMC), CTA_{mic}^+ does not affect the equilibrium point of the reaction (Figure S6), thus $[CTA_{mic}^+]$ turns out to have zero order. This behavior is expected as each micelle can accommodate multiple $AuBr^{2-}$ ions (Figure 1c in the main text). Equation (S1) now can be re-written as follows:

$$E^{o\prime}_{CTA_{mic}AuBr_2/AuNP} = E^{\circ}_{Fe^{3+}/Fe^{2+}} - \frac{RT}{zF}\ln\frac{[Fe^{2+}]^2}{[Fe^{3+}][Br^-]^2} \qquad (S2)$$

To determine the standard reduction potential, we replace the concentrations in equation (S1) by activities of involved species. Since CTA_{mic}^+ does not affect the equilibrium point of the reaction (Figure S6), we do not include its activity. Now, the standard reduction potential is determined as follows:

$$E^{o}_{CTA_{mic}AuBr_2/AuNP} = E^{\circ}_{Fe^{3+}/Fe^{2+}} - \frac{RT}{zF}\ln\frac{\alpha_{CTA_{mic}AuBr_2}\alpha_{Fe^{2+}}}{\alpha_{Fe^{3+}}\alpha^2_{Br^-}}$$

Where α_i is the activity of species i (i stands for the involved species above). Using the relationship between activity and concentration, $\alpha_i = \gamma_i\frac{C_i}{C_i^\circ}$ (γ_i: activity coefficient, C_i: effective concentration, C_i° : standard state concentration), the equation above now becomes:

$$E^{o}_{CTA_{mic}AuBr_2/AuNP} = E^{\circ}_{Fe^{3+}/Fe^{2+}} - \frac{RT}{zF}\ln\frac{\gamma_{CTA_{mic}AuBr_2}[CTA_{mic}AuBr_2]\gamma_{Fe^{2+}}[Fe^{2+}]}{\gamma_{Fe^{3+}}[Fe^{3+}]\gamma^2_{Br^-}[Br^-]^2} \qquad (S3)$$

Using the equation of the Debye-Hückel theory, the activity coefficient of each ion i can be estimated as follows:

$$\log\gamma_i = \frac{Az_i^2\sqrt{I}}{1 + Ba_{0,i}\sqrt{I}}$$

Where z_i represents the charge number of ion i, and $a_{0,i}$ is the effective ionic radius. A and B are parameters that vary with the temperature and the dielectric constant of the solvent. For an aqueous solution at 25 °C, the values A and B are 0.511 and 0.329, respectively. I is the ionic strength of the solution and can be calculated using the following equation:

$$I = \frac{1}{2}\sum_i z_i^2\left(\frac{C_i}{C^0}\right)$$

Using the concentrations listed for every species in the experimental protocols, the ionic strength of each solution is approximately 0.013. Note that, in this ionic strength calculation, the contribution of surfactant micelles is ignored as they do not fully behave like an electrolyte. The main contributors are HCl (0.01M), $FeCl_3$ (0.267mM), and CTAB (1mM, as the critical micelle concentration). Other chemical species have much lower concentrations, which were not considered in the ionic strength calculation. Using this value, the activity coefficient for each species from equation (S3) was determined and summarized in Table S2.

Table S2. The activity coefficients tabulated for each reactant and product in chemical equation 4.

Species	z_i	$a_{0,i}$ (Å)[a]	γ_i
Fe^{3+}	3	9.0	0.41
Fe^{2+}	2	6.0	0.65
CTA^+	1	30[b]	0.94
Br^-	-1	3.0	0.89
$AuBr_2^-$	-1	1.4	0.89
$CTA_{mic}AuBr_2$	-	-	0.91

(a) Values obtained from Speight[6]
(b) Approximated from the radius of a CTAB micelle.[7]

Since the $CTA_{mic}AuBr_2$ complex does not significantly dissociate in solution, the mean activity coefficient is obtained using the geometric mean equation:

$$\gamma_{\pm} = \sqrt[(x+y)]{\gamma_+^x \gamma_-^y}$$

Where $\gamma_{\pm}$ is the mean activity coefficient, γ_+ and γ_- are the activity coefficients of the cation and anion, respectively. The values x and y are the stoichiometric coefficients of the cation and anion, respectively.

It is worth noting that the ionic strength and activity coefficient are strongly affected by ions with greater charge. For this reason, the activity coefficients of Fe^{3+} and Fe^{2+} have deviated far more from unity than Br^- and $CTA_{mic}AuBr_2$. Although these deviations appear substantial, $E^{0\prime}_{CTA_{mic}AuBr_2/AuNP}$ is only larger than $E^{0}_{CTA_{mic}AuBr_2/AuNP}$ by 0.016V (see Table S3). This is due to the logarithmic operator on the ratio of the activities in the Nernst equation. Besides, the 0.016V difference is similar across all nanoparticle sizes due to our calculation for the activities above.

Table S3. Comparison between formal reduction potentials ($E^{0\prime}_{CTA_{mic}AuBr_2/AuNP}$) obtained from equation (S2) and standard reduction potentials ($E^{0}_{CTA_{mic}AuBr_2/AuNP}$) obtained equation (S3).

Gold nanoparticle diameter (nm)	$E^{0\prime}_{CTA_{mic}AuBr_2/AuNP}$ (V)	$E^{0}_{CTA_{mic}AuBr_2/AuNP}$(V)	$E^{0\prime} - E^{0}$(V)
5.0	0.665	0.649	0.016
8.7	0.709	0.693	0.016
10.2	0.734	0.718	0.016
31.9	0.770	0.755	0.016
50	0.762	0.746	0.016
73	0.773	0.757	0.016

+ Determination of formal reduction potential $E^{o\prime}_{AuBr_2^-/AuNP}$ and standard reduction potential $E^{o}_{AuBr_2^-/AuNP}$

When we need to determine the standard reduction potentials of gold particles in which $AuBr_2^-$ is the oxidized product. We focus on the specific equilibrium below and use Nernst equation for the associated compounds:

$$Au_n^{NP}(s) + Fe^{3+} + 2Br^- \rightleftharpoons Au_{n-1}^{NP}(s) + Fe^{2+} + AuBr_2^-$$

The half-cell reaction for oxidation: $Au_n^{NP}(s) + 2Br^- \rightarrow 1e^- + Au_{n-1}^{NP}(s) + AuBr_2^-$

The half-cell reaction for reduction: $Fe^{3+} + 1e^- \rightarrow Fe^{2+}$

Using the Nerst equation as in the above case, we have:

$$E^{\circ,}_{AuBr_2^-/AuNP} = E^{\circ}_{Fe^{3+}/Fe^{2+}} - \frac{RT}{zF}\ln\frac{[AuBr_2^-][Fe^{2+}]}{[Fe^{3+}][Br^-]^2} \qquad (S4)$$

Note that we still need to account for all other chemical equilibria mentioned in the main text. From equation (3) in the main text, $[AuBr_2^-] = \frac{[CTA_{mic}AuBr_2]}{K_m[CTA_{mic}^+]}$, substituting this $[AuBr_2^-]$, having zero order for $[CTA_{mic}^+]$, and assuming $[CTA_{mic}AuBr_2]$ is equal to $[Fe^{2+}]$, we obtain the below equation from S4:

$$E^{\circ,}_{AuBr_2^-/AuNP} = E^{\circ}_{Fe^{3+}/Fe^{2+}} - \frac{RT}{zF}\ln\frac{[Fe^{2+}]^2}{K_m[Fe^{3+}][Br^-]^2}$$

When using activities for all species, we have:

$$E^{\circ}_{AuBr_2^-/AuNP} = E^{\circ}_{Fe^{3+}/Fe^{2+}} - \frac{RT}{zF}\ln\frac{\gamma_{CTA_{mic}AuBr_2}[CTA_{mic}AuBr_2]\gamma_{Fe^{2+}}[Fe^{2+}]}{K_m\gamma_{Fe^{3+}}[Fe^{3+}]\gamma_{Br^-}^2[Br^-]^2}$$

+ Determination of $E^o_{Au^+/AuNP}$

Similarly, when we need to determine the standard reduction potentials of gold particles in which Au^+ is the oxidized product. We focus the specific equilibrium below and use Nernst equation for the involved compounds:

$Au_n^{NP}(s) + Fe^{3+} \rightleftharpoons Au_{n-1}^{NP}(s) + Fe^{2+} + Au^+$ (same as equation (1) in the main text)

The half-cell reaction for oxidation: $Au_n^{NP}(s) \rightarrow 1e^- + Au_{n-1}^{NP}(s) + Au^+$

The half-cell reaction for reduction: $Fe^{3+} + 1e^- \rightarrow Fe^{2+}$

Using the Nernst equation as in the two above cases, we have:

$$E^{\circ}_{Au^+/AuNP} = E^{\circ}_{Fe^{3+}/Fe^{2+}} - \frac{RT}{zF}\ln\frac{[Au^+][Fe^{2+}]}{[Fe^{3+}]}$$

From equation (2) in the main text, $[Au^+] = \frac{[AuBr_2^-]}{\beta[Br^-]^2}$, substituting this term into the above Nernst equation, we have:

$$E^{\circ,}_{Au^+/AuNP} = E^{\circ}_{Fe^{3+}/Fe^{2+}} - \frac{RT}{zF}\ln\frac{[AuBr_2^-][Fe^{2+}]}{\beta[Br^-]^2[Fe^{3+}]}$$

From equation (3) in the main text, $[AuBr_2^-] = \frac{[CTA_{mic}AuBr_2]}{K_m[CTA_{mic}^+]}$, substituting this term into the above equation and assuming a zero order for $[CTA_{mic}^+]$ and $[CTA_{mic}AuBr_2]$= $[Fe^{2+}]$, we have:

$$E^{\circ\prime}_{Au^+/AuNP} = E^{\circ}_{Fe^{3+}/Fe^{2+}} - \frac{RT}{zF}\ln\frac{[Fe^{2+}]^2}{K_m\beta[Fe^{3+}][Br^-]^2}$$

When using activities for all species, we have:

$$E^{\circ}_{Au^+/AuNP} = E^{\circ}_{Fe^{3+}/Fe^{2+}} - \frac{RT}{zF}\ln\frac{\gamma_{CTA_{mic}AuBr_2}[CTA_{mic}AuBr_2]\gamma_{Fe^{2+}}[Fe^{2+}]}{K_m\beta\gamma_{Fe^{3+}}[Fe^{3+}]\gamma_{Br}^2-[Br^-]^2}$$

This is equation (6) in the main text, which can be used to determine the standard reduction potential for Au^+/AuNP redox couple. As we compare equation (6) to (S3), we know that $E^{\circ\prime}_{Au^+/AuNP}$ is also higher than $E^{\circ}_{Au^+/AuNP}$ about 0.016V across all particle sizes.

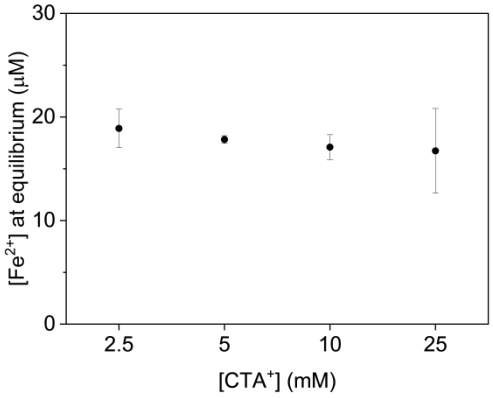

Figure S6. Measured $[Fe^{2+}]$ at equilibrium of the reaction between 31.7 nm gold nanoparticles and Fe^{3+} where $[CTA^+]$ is above the CMC and varies in a range up to one order of magnitude. The difference in $[Fe^{2+}]$ is insignificant across control samples with various $[CTA^+]$.

Calculating molar volume from Au-Au interatomic distance in gold nanoparticles

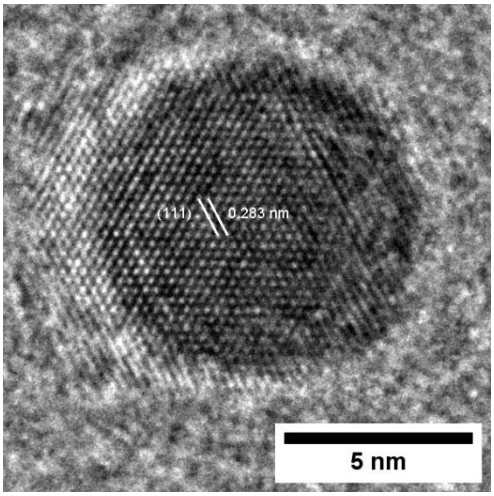

Figure S7. HRTEM image of an individual gold nanoparticle with a diameter of 8.6 nm.

The molar volume of the gold nanoparticles was estimated from the Au-Au interatomic distance. This distance was taken from the measured interplanar distance shown in Figure S7. The interatomic distance was measured for 37 lattice fringes, which yielded an average interatomic distance of 0.283 nm. To compute the uncertainty, it was taken into account the HR-TEM information limit 0.18 nm and divided this by 37, resulting in a 0.005 nm uncertainty. This result shows that our measured interatomic distance is 0.283 nm ± 0.005 nm for the 8.6 nm gold nanoparticle, and is about 1.74% smaller than the Au-Au separation (0.288 nm) in bulk gold.[6]Assuming the lattice contraction is uniform throughout the entire nanoparticle, the interatomic distance was then used to calculate the effective atomic volume ($V_{Au,eff}$), which represents the actual volume occupied by the gold atoms in a crystalline solid. The effective volume is calculated as follows

$$V_{Au,eff} = \frac{1}{4}(2\sqrt{2}r)^3 \qquad \text{(S5)}$$

Where the radius (r) is taken to be half the interatomic distance. Here, the effective volume is 25% of the unit cell volume, which is $(2\sqrt{2}r)^3$ for a face-centered cubic crystal configuration. Finally, the molar volume (V_M) is obtained using

$$V_M = V_{Au,eff} N_A \qquad \text{(S6)}$$

Where N_A is Avogadro's constant.

Using equations (S5) and (S6), we obtain a molar volume of 9.56×10^{-6} m^3mol^{-1} from an interatomic distance of 0.283 nm in an ~8 nm gold nanoparticle. This represents a 6.3% reduction in molar volume in comparison to the bulk value of 1.021×10^{-5} m^3 mol^{-1} and suggests a small amount of lattice contraction in gold nanoparticles.

Estimation of K_m values to calculate the redox potentials of gold nanoparticles

To calculate the approximate value of K_m for further reduction potential measurements of gold nanoparticles using equations (5) and (6), we first assumed the redox potential of 31.9 and 73 nm nanoparticles to be those of predicted by Plieth's equation (equation 7 in the main text)

Therefore, the redox potentials of 31.9 nm and 73 nm gold nanoparticles can be calculated as

$$E^{\circ}_{Au^+/AuNP(31.9\ nm)} = E^{\circ}_{Au^+/Au(bulk)} - \frac{2\gamma V_M 1}{zF\ r} = 1.805\ V\ vs\ SHE$$

$$E^{\circ}_{Au^+/AuNP(73\ nm)} = E^{\circ}_{Au^+/Au(bulk)} - \frac{2\gamma V_M 1}{zF\ r} = 1.819\ V\ vs\ SHE$$

These redox potential values are used in the Nernst equation (6)

$$E^{\circ}_{Au^+/AuNP(31.9\ nm)} = 1.805\ V = E^{\circ}_{Fe^{3+}/Fe^{2+}} - \frac{RT}{zF}\ln\frac{\gamma_{CTA_{mic}AuBr_2}[CTA_{mic}AuBr_2]\gamma_{Fe^{2+}}[Fe^{2+}]}{K_m\beta\gamma_{Fe^{3+}}[Fe^{3+}]\gamma^2_{Br^-}[Br^-]^2}$$

$$E^{\circ}_{Au^+/AuNP(73\ nm)} = 1.819\ V = E^{\circ}_{Fe^{3+}/Fe^{2+}} - \frac{RT}{zF}\ln\frac{\gamma_{CTA_{mic}AuBr_2}[CTA_{mic}AuBr_2]\gamma_{Fe^{2+}}[Fe^{2+}]}{K_m\beta\gamma_{Fe^{3+}}[Fe^{3+}]\gamma^2_{Br^-}[Br^-]^2}$$

Where $E^{\circ}_{Fe^{3+}/Fe^{2+}} = 0.771$ V vs SHE, and the concentration and activity coefficient terms are known from experiments.

Hence, the estimated K_m of 6×10^5 and 9×10^5 M were achieved for the 31.9 and 73 nm gold nanoparticles, respectively. Detailed calculation for the 31.9 nm is illustrated as following:

$[Fe^{2+}]_{at\ equilibrium} = 1.93 \times 10^{-5}$ M, determined by phenanthroline assay

$[Fe^{3+}]_{at\ equilibrium} = [Fe^{3+}]_{initial} - [Fe^{2+}]_{at\ equilibrium} = 2.52 \times 10^{-4}$ M - 1.93×10^{-5} M = 2.33×10^{-4} M

$[Au^+]_{at\ equilibrium} = [Fe^{2+}]_{at\ equilibrium} = 1.93 \times 10^{-5}$ M

$[Br^-]_{at\ equilibrium} = [Br^-]_{initial} - 2 \times [Au^+]_{at\ equilibrium} = 1.10 \times 10^{-3}$ M – ($2 \times 1.93 \times 10^{-5}$ M) = 1.06×10^{-3} M

Given the estimations, we tested five K_m values within the range from 5×10^5 to 13×10^5 (2×10^5 step) using equation (6) along with the experimental concentrations, and fit these data to a A-B/*d* function (*d* is the nanoparticle diameter) and extrapolated $E^{\circ}_{Au^+/AuNP}$ to the bulk value for each K_m value. The resulting values from such extrapolations are summarized in Table S4. Similarly, the same calculation was done for $E^{\circ}_{AuBr_2^-/AuNP}$.

Table S4. Scanning over different K_m values and extrapolating the $E^{\circ}_{Au^+/AuNP}$ to $E^{\circ}_{Au^+/Au(bulk)}$.

K_m (x 10^5)	$E^{\circ}_{Au^+/Au(bulk)}$ extrapolation (V vs SHE) (Fit follows $y = A - \frac{B}{d}$)
5	1.82
7	1.82
9	1.83
11	1.84
13	1.84

From the results in Table S2, the fitting curve with $K_m = 9 \times 10^5$ give the closest prediction of 1.83V (vs SHE) for $E^{\circ}_{Au^+/Au(bulk)}$. This K_m was used in equation (6) to give the standard redox potential of nanoparticles at different sizes as described in Figure 2 c & d in the main text.

Charging effects on the reduction potentials

The amount of charge on a metallic nanoparticle can affect its reduction potential. This charge is typically accumulated (or dissipated) during the synthesis or post-synthesis of nanoparticles, or the reactions between the particles and other chemical species.[8] The stored electrons raise the Fermi level and lower the reduction potential of the nanoparticle. The degree of this change can be factored into Plieth's equation to predict the reduction potential of charged particles[9, 10], as follows

$$E^{\circ}_{Au^+/AuNP} = E^{\circ}_{Au^+/Au(bulk)} - \frac{2\gamma V_M 1}{zF\ r} + \frac{V_M}{8\pi F r^4} \frac{z^2 e^2}{4\pi\varepsilon_0 \varepsilon_r} \qquad (S7)$$

Where z is the number of charges on each nanoparticle, ε_0 is the vacuum permittivity ($8.85 \times 10^{-12} F/m$), ε_r is the relative permittivity of the surrounding medium. Keep in mind that the sign on the last term will change depending on if the stored charge is positive or negative.

Using equation (S7), the standard reduction potentials for 5 nm – 100 nm gold nanoparticles with charges anywhere between 0 – 10,000 e were calculated and summarized in Figure S8.

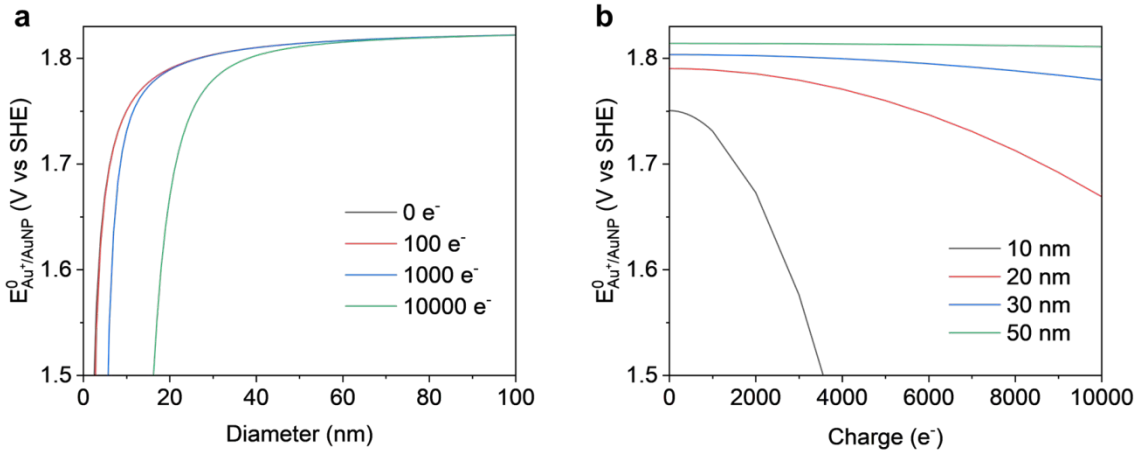

Figure S8. (a) The calculated reduction potentials of neutral (0 e^-) and charged (100 e^-, 1,000 e^- and 10,000 e^-) gold nanoparticles are plotted for their diameters from 5 nm to 100 nm. Note, the curves representing 0 e^-, and 100 e^- overlap with one another due to insignificant variation in the reduction potentials. (b) The calculated reduction potentials of gold nanoparticles plotted for 10 nm, 20 nm, 30 nm, and 50 nm gold nanoparticles with increasing charge.

From these results, we can draw two key conclusions. First, a significant amount of negative charge (i.e., electrons) is necessary to lower the reduction by several millivolts. Approximately, 150 e^- are needed to shift the reduction potential of a 10 nm gold nanoparticle by 1 mV. Second, the magnitude of the charging effect is dependent on particle size, being less prominent in large nanoparticles. From the calculated values shown in Table S5, a 20 nm nanoparticle would require up to 1,000 e^- to shift its potential by 1 mV, while a 30 nm nanoparticle would require an order of 10,000 e^- to observe a significant effect.

Table S5. Selected calculated standard reduction potentials of neutral and charged gold nanoparticles of different diameters.

Diameter (nm)	Charge (e^-)	Standard Reduction Potential (V vs SHE)
10	0	1.750
	10	1.750
	100	1.750
	1000	1.731
	5000	1.266
20	0	1.790
	10	1.790
	100	1.790
	1000	1.789
	5000	1.760
30	0	1.803
	10	1.803
	100	1.803
	1000	1.803
	5000	1.797

With these charging effects in mind, we performed a charge titration to estimate the total number of stored electrons in 11.9 nm gold nanoparticles. We used thionine due to its well separated absorbance peak (600 nm) from the LSPR of our gold nanoparticles and large molar absorptivity (Figure S9a). Furthermore, thionine in its reduced form is colorless, therefore its absorbance decreases as it accepts electrons from the particles. However, the amount of charge was found to be too small for this effect to be observed from a single addition of thionine, thus we opted to perform a titration curve as shown in Figure S9b. Thus, from the intercept we determined that 0.055 μM of thionine was reduced after the addition of the first aliquot. Using this extrapolated concentration, we calculated a maximum storage of about 38 electrons per gold nanoparticle. Note, the number of gold nanoparticles in our solution was determined from the absorbance at the LSPR (before adding thionine) and its molar extinction coefficient (2.04×10^8 M^{-1} cm^{-1}). According to our calculations using equation (S7), this amount of charge would account for <1 mV shift in 11.9 nm gold nanoparticles. Assuming the charge density is consistently similar across all other nanoparticle sizes, charge is not a significant factor in determining the reduction potentials of our nanoparticles in this study.

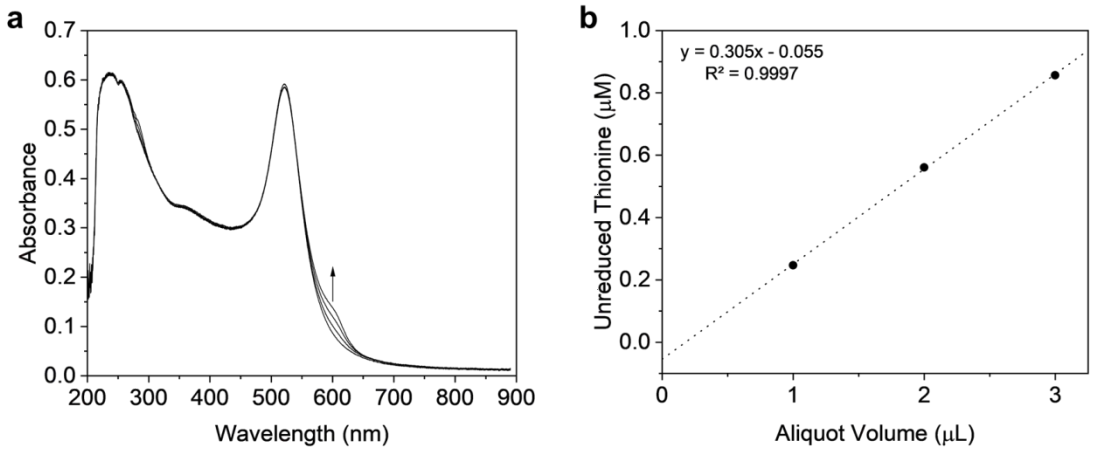

Figure S9. (a) Titration of excess charge in 11.9 nm gold nanoparticles using 1 μL aliquots of thionine dye (~0.6 mM). After each addition of thionine, an absorbance peak at 600 nm emerges (indicated by the arrow). (b) A titration curve corresponding to the final concentration of thionine after each aliquot. The absorbance of the pure gold nanoparticles was subtracted from the thionine absorbance at 600 nm.

Reference

(1) Zheng, Y. Q.; Zhong, X. L.; Li, Z. Y.; Xia, Y. N. Successive, Seed-Mediated Growth for the Synthesis of Single-Crystal Gold Nanospheres with Uniform Diameters Controlled in the Range of 5-150 nm. *Particle & Particle Systems Characterization* **2014**, *31* (2), 266-273. DOI: 10.1002/ppsc.201300256.
(2) Yoon, S.; Kim, C.; Lee, B.; Lee, J. H. From a precursor to an etchant: spontaneous inversion of the role of Au(iii) chloride for one-pot synthesis of smooth and spherical gold nanoparticles. *Nanoscale Advances* **2019**, 10.1039/C9NA00157C. DOI: 10.1039/C9NA00157C.
(3) Mao, Z.; Espinoza, R.; Garcia, A.; Enwright, A.; Vang, H.; Nguyen, S. C. Tuning Redox Potential of Gold Nanoparticle Photocatalysts by Light. *ACS Nano* **2020**, *14* (6), 7038-7045. DOI: 10.1021/acsnano.0c01704.
(4) Zou, R.; Guo, X.; Yang, J.; Li, D.; Peng, F.; Zhang, L.; Wang, H.; Yu, H. Selective etching of gold nanorods by ferric chloride at room temperature. *CrystEngComm* **2009**, *11* (12), 2797-2803, 10.1039/B911902G. DOI: 10.1039/B911902G.
(5) Hendel, T.; Wuithschick, M.; Kettemann, F.; Birnbaum, A.; Rademann, K.; Polte, J. In Situ Determination of Colloidal Gold Concentrations with UV–Vis Spectroscopy: Limitations and Perspectives. *Analytical Chemistry* **2014**, *86* (22), 11115-11124. DOI: 10.1021/ac502053s.
(6) James Speight, P. D. *Lange's Handbook of Chemistry, Sixteenth Edition*; McGraw-Hill Education, 2005.
(7) Park, K.; Koerner, H.; Vaia, R. A. Depletion-Induced Shape and Size Selection of Gold Nanoparticles. *Nano Letters* **2010**, *10* (4), 1433-1439. DOI: 10.1021/nl100345u.
(8) Mulvaney, P. Surface Plasmon Spectroscopy of Nanosized Metal Particles. *Langmuir* **1996**, *12* (3), 788-800. DOI: 10.1021/la9502711.
(9) Lee, D.-K.; Park, S.-I.; Lee, J. K.; Hwang, N.-M. A theoretical model for digestive ripening. *Acta Materialia* **2007**, *55* (15), 5281-5288. DOI: https://doi.org/10.1016/j.actamat.2007.05.048.
(10) Scanlon, M. D.; Peljo, P.; Méndez, M. A.; Smirnov, E.; Girault, H. H. Charging and discharging at the nanoscale: Fermi level equilibration of metallic nanoparticles. *Chemical Science* **2015**, *6* (5), 2705-2720, 10.1039/C5SC00461F. DOI: 10.1039/C5SC00461F.